Electrodeposition of Nickel Hydroxide Nanoparticles on Carbon Nanotube Electrodes: Correlation of Particle Crystallography with Electrocatalytic Properties

Sharel P. E,[†] *Danqing Liu,*[†] *Robert A. Lazenby,*[†] *Jeremy Sloan,*[‡] *Marcio Vidotti,*[§] *Patrick R. Unwin*[*†] *and Julie V. Macpherson.*[*†]

[†]Department of Chemistry and [‡]Department of Physics, University of Warwick, Coventry, CV4 7AL, United Kingdom

[§]Departamento de Química, Universidade Federal do Paraná, CP 19032, CEP 81531-980 Curitiba, PR, Brazil

* To whom correspondence should be addressed. E-mail: p.r.unwin@warwick.ac.uk (P.R. Unwin), j.macpherson@warwick.ac.uk (J.V. Macpherson).

KEYWORDS. Nanostructured Electrodes, Nickel Hydroxide, Carbon Nanotubes, Electrocatalysis, Methanol Oxidation, Ethanol Oxidation

ABSTRACT

The use of two different electrodeposition approaches to form nickel hydroxide, $Ni(OH)_2$, nanoparticles (NPs) of different crystallographic orientations on single-walled carbon nanotubes is demonstrated via: (i) the electrochemical generation of OH^- (~ mM), in the presence of Ni^{2+}, resulting in the formation of disordered α-phase $Ni(OH)_2$ NPs by precipitation (direct approach); (ii) the electrodeposition of Ni NPs that are converted to $Ni(OH)_2$ through potential cycling in alkaline media to form the more thermodynamically favourable, ordered β-phase $Ni(OH)_2$ NPs (indirect approach). NPs produced by the direct approach exhibit remarkable electrocatalytic activity towards both methanol and ethanol oxidation, exhibiting excellent specific activities (SA) of ~2.8 kA g^{-1} for 0.5 M methanol and ~3.7 kA g^{-1} for 0.5 M ethanol. In contrast, NPs produced by the indirect approach shows SA values about an order of magnitude lower. This study demonstrates the capability of electrochemistry for the tailored synthesis of $Ni(OH)_2$ nanostructures for electrocatalytic applications, and a powerful, but simple, combinatorial approach for quick activity screening.

INTRODUCTION

The electrocatalytic oxidation of small organic molecules has attracted considerable interest for applications in different areas of electrochemical science, such as fuel cells[1] and electrochemical-based sensors.[2] Among these the electrochemical oxidation of methanol (MeOH) and ethanol (EtOH) have been active areas of research, especially to aid the development (and understanding) of direct alcohol-based fuel cells.[3] The most widely used catalysts for the alcohol oxidation reaction (AOR) are rather expensive and scarce metals such as platinum[4] and ruthenium.[5] There is thus a need to find alternative, cheaper materials, which perform as well, if not better, in terms of electrocatalytic activity.

Nickel hydroxide ($Ni(OH)_2$) is one such material that exhibits high electrochemical activity and cost effectiveness, and so this electrode has been the focus of considerable attention.[6-10] A variety of different synthetic routes are available for the production of a wide range of different $Ni(OH)_2$ morphologies.[7, 11] The electrocatalytic activity of $Ni(OH)_2$ results from the oxidized form, Ni(OOH), owing to unpaired d electrons or empty d-orbitals[12-14] which are available to bond with adsorbed species and intermediates.

It is well known that the electrocatalytic activity of materials can be increased significantly when nanostructures, such as nanoparticles (NPs), are employed.[15-16] Among electrocatalytic supports, carbon nanotubes (CNTs) have been shown to be extremely attractive for metal NPs[17-18] and metal oxides[19] due to their exceptional intrinsic properties, such as chemical stability[20] and nanoscale dimensions.[21] Moreover, compared to the more traditional support materials, such as carbon black, CNTs have been shown to offer an increased porosity and enhancement of the kinetic rate constant for the electrocatalytic process of interest (for similar metal NP loadings and carbon surface areas).[22-24] Several approaches have been adopted for depositing metal NPs onto

nanotube electrodes, such as sol gel,[25] sonochemistry,[26] and hydrothermal methods.[27] However, these methods can be time-consuming and challenging to use. In contrast, electrochemistry is both rapid and facile, and a good deal of control over the nucleation and growth of metal NPs can be achieved by varying the deposition potential and time.[28-29]

The fabrication of $Ni(OH)_2$/CNT composite materials has often involved dispersing CNTs in solution followed by chemical precipitation of $Ni(OH)_2$.[30-31] The typical methods for CNT growth are arc discharge,[32] laser ablation[33] and catalyzed chemical vapor deposition (cCVD).[34] Material produced by the first two methods has mainly been used in electrochemistry, but this contains large amounts of metal NPs and amorphous carbon, making the use of a clean-up procedure after growth mandatory.[35-36] However, CNTs contain significant amount of metallic impurities, even after extensive purification processes,[37] and these clean-up procedures introduce considerable defects in the single-walled carbon nanotubes (SWNTs).[38] The electrochemical behavior of redox systems can be strongly affected by such impurities and defects, which are particularly problematic for fundamental studies of eletrocatalysis.[39] In contrast, CNTs grown using cCVD method have been shown to exhibit low defect density,[40] high crystallinity and are relatively free of metallic NPs.[41]

In principle, $Ni(OH)_2$ NP deposition can be driven electrochemically using two approaches: (i) the *direct approach*[42-46] where $Ni(OH)_2$ is precipitated from highly supersaturated solutions by electrochemically generating high concentrations of OH^- at the electrode/electrolyte interface, in the presence of Ni^{2+}; and: (ii) the *indirect approach*, whereby Ni NPs are first electrodeposited by direct reduction of Ni^{2+} and subsequently electrochemically converted to $Ni(OH)_2$ by potential cycling in a basic electrolyte.[47-49] In this paper we compare the two different procedures for $Ni(OH)_2$ NP deposition on SWNT electrodes in terms of both the resulting crystalline phase

of the $Ni(OH)_2$ and electrocatalytic performance towards the EtOH oxidation reaction (EOR) and MeOH oxidation reaction (MOR).

The $Ni(OH)_2$/SWNTs are electrochemically interrogated using the microcapillary electrochemical method (MCEM),[28] which allows multiple electrochemical measurements to be made in different locations on the same electrode, thereby allowing a range of key parameters to be changed and investigated, without the need to make new electrodes and with minimal processing of the SWNTs. Although, SWNTs are attracting considerable attention as a support for electrocatalytic materials,[22, 49-50] in the vast majority of cases, SWNT/NP composites are assessed by immobilizing, or producing, these structures on an electrode (typically glassy carbon)[49, 51-52] which has its own intrinsic electroactivity. In contrast, our approach examines the behavior of the SWNT/NP materials alone and thus circumvents any problems and contributions that may arise from the need to use a further electrode support.

EXPERIMENTAL METHODS

SWNT Network Growth and Electrode Preparation: High density (HD) SWNT networks were used to provide a relatively large surface area for NP electrodeposition. The HD SWNT networks were grown on 2 cm × 2 cm insulating Si/SiO_2 substrates (IDB Technologies Ltd., n-type, 525 μm thickness with 300 nm of thermally grown SiO_2 on both sides), using cCVD, with cobalt (Co)[53] NPs as the catalyst and EtOH as a carbon source.[54] A side contact to the SWNT networks (for subsequent electrochemical measurements) was made by evaporating Cr (3 nm)/Au (60 nm) through a shadow mask using a Moorfields MiniLab deposition system (Moorfield Associates).

Electrodeposition of $Ni(OH)_2$ on SWNT Network Electrodes: All aqueous solutions were prepared using high purity Milli-Q reagent water (Millipore Corp.) with a resistivity of 18.2 MΩ cm at 25 °C. 10 mM nickel nitrate ($Ni(NO_3)_2$, Aldrich, 99.999%) and 10 mM nickel sulphate ($NiSO_4$, Aldrich, 99%) solutions were used for the electrodeposition of $Ni(OH)_2$ NPs for the direct and indirect approach, respectively, using a droplet method (Figure 1a).[55] Electrochemical measurements were carried out in a 3-electrode setup, with the SWNT network acting as the working electrode. Electrical contact to the Au band side contact was made via a pin. A drop of electrolyte solution (~15 µL, 4 mm diameter) was placed on the electrode surface, fairly close to the gold band but without making contact (Figure 1a). A platinum wire was used as a counter electrode (CE). On the timescale of electrodeposition procedure (5 seconds) there is little chance of any CE products reaching the working electrode (which is located at least 1 mm away from the end of the CE). AgCl-coated Ag wire acted as a quasi-reference electrode (QRCE), against which all potentials are quoted. This QRCE was found to be sufficiently stable under the experimental conditions and timescale.[56-57] Both the Pt CE and AgCl-coated Ag wire QRCE were positioned within the droplet of solution to complete the circuit.

For the direct approach, precipitation of $Ni(OH)_2$ on the SWNT network electrode occurred by driving the electroreduction of nitrate (from dissolved $Ni(NO_3)_2$) at the SWNT electrode to form OH^- locally (equation 1).

$$NO_3^- + 7H_2O + 8e^- \rightleftharpoons NH_4^+ + 10OH^- \quad (1)$$

This concept is illustrated schematically in Figure 1b.[58] To produce NPs it was necessary to produce a high concentration of OH^-, leading to a highly supersaturated solution. This was achieved by driving the reduction process (1) at a negative driving potential of -1.5 V *vs.* Ag/AgCl, for 5 s. From the resulting current-time transient it is possible to determine the OH^-

concentration near the electrode surface;[12] ~ mM, as described in Electronic Supporting Information (**ESI**), **Section 1**.

For the indirect approach, Ni metal NPs were first electrodeposited by applying a sufficiently negative reduction potential of -1.5 V *vs*. Ag/AgCl, for 5 s, in $NiSO_4$ solution, followed by oxidative potential cycling (+0.1 V to +0.5 V at 5 mV s^{-1} for 10 cycles) in 0.1 M KOH (Aldrich).

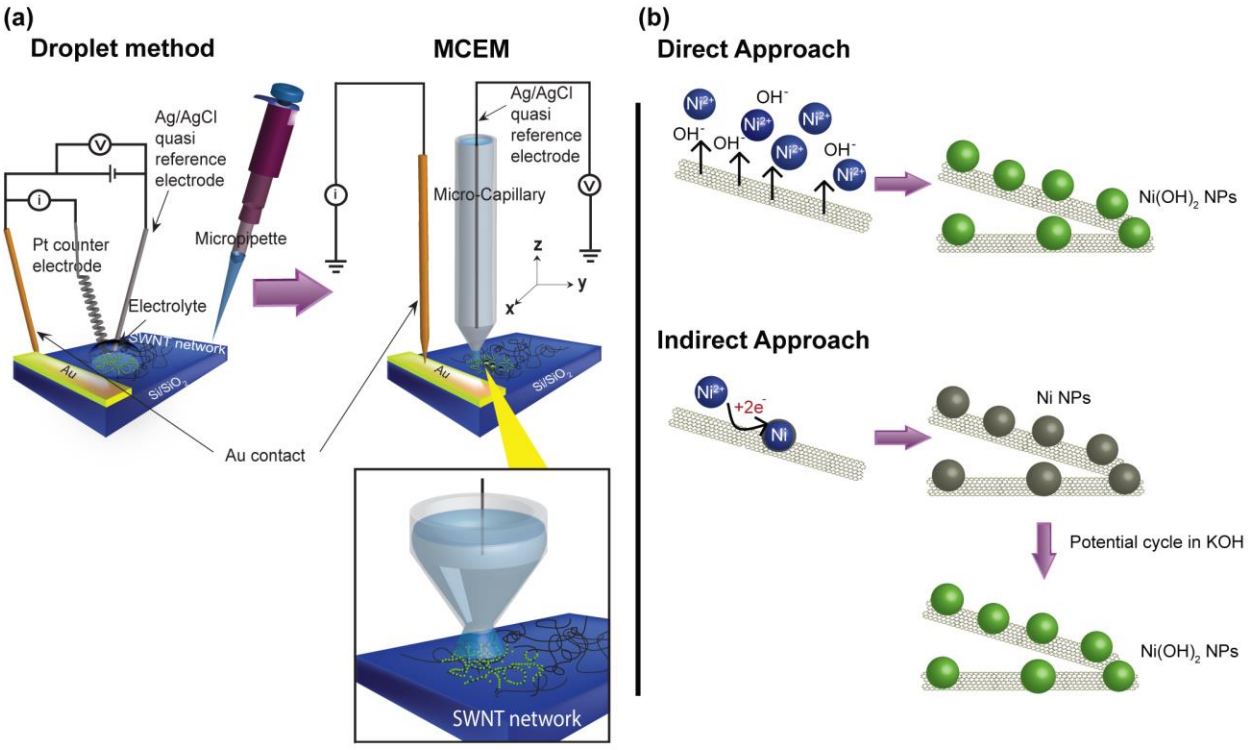

Figure 1. Experimental set-up for (a) the electrodeposition of NPs using the droplet method and microscopic electrocatalytic measurements using the MCEM. (b) Illustration showing $Ni(OH)_2$ NPs formation on a SWNT network electrode by both the direct (top) and indirect (bottom) approach.

Material characterization: Bare and functionalized SWNT networks were characterized using both field-emission scanning electron microscopy (FE-SEM: Zeiss Supra 55-VP, 1 kV

acceleration voltage) and atomic force microscopy (AFM: tapping mode, Bruker-Nano Enviroscope). Micro-Raman spectra were recorded using a Renishaw inVia Raman microscope (514.5 nm Ar laser, 10 mW). For these techniques, three measurements (n = 3) were recorded per substrate. For high resolution transmission electron microscopy (HR-TEM) sample preparation, $Ni(OH)_2$ NPs were mechanically scratched from the growth substrate using a blade and dispersed in absolute EtOH (Fisher Scientific) solution. The suspension underwent sonication for 4 minutes and centrifugation for 15 minutes (Eppendorf, 10 000 rpm) to cause particle sedimentation. A drop of solution (3 µL), containing the sedimented particles, was then placed onto a lacey carbon TEM grid (Agar Scientific) and left until the EtOH had evaporated. HR-TEM was conducted (n = 3) using a JEM 2100 TEM (JEOL, LaB_6 filament, operated at 200 kV) equipped with energy-dispersive X-ray spectroscopy (EDS) and selected area electron diffraction (SAED) technique.

Electrocatalytic Measurements: 0.5 M MeOH (VWR, 99%) and 0.5 M EtOH (Fisher, 99.5%) were used for MOR and EOR, respectively, in 0.1 M KOH. All chemicals were used as received. Electrochemical measurements were performed using the MCEM, a localized electrochemical technique which has been described in detail previously.[28, 59] The electrochemical cell consisted of a borosilicate glass capillary (1.2 mm outer diameter, 0.69 mm internal diameter, Harvard Apparatus Ltd.), pulled to a sharp tip using a laser pipet puller (P-2000, Sutter Instrument Co.). The end was polished to reveal an aperture in the range 60 – 62 µm (measured using optical microscopy for each capillary) and rendered hydrophobic on the outer walls through immersion in dichlorodimethylsilane (Fisher, ≥99%) for 90 s, with high purity Ar gas flowing through the capillary to prevent any internal silanization. The capillary was filled with the solution of interest and a Ag/AgCl wire as QRCE was inserted. The SWNT-$Ni(OH)_2$ substrate was connected as the

working electrode and the capillary was manually lowered towards the electrode using an *x-y-z* micropositioner (Newport 433 series), with the aid of a camera (PixeLINK PL-B776U). A quick tap was applied to the micropositioner, once the capillary was close to the sample surface, so that an electrolyte meniscus formed on the SWNT network, without the capillary itself making contact with the electrode surface. Electrochemical measurements were made in a 2-electrode arrangement (due to the small currents, < 120 nA), for which the use of a QRCE gives adequate stability,[60-61] using a potentiostat (CH Instruments, Austin, TX; model 730A).

RESULTS AND DISCUSSION

$Ni(OH)_2$ Formation on SWNT Network Electrodes. Typical FE-SEM and AFM images shown in Figures 2a and 2b, respectively, are of a representative pristine (bare) HD SWNT network with a measured SWNT density >>10 μm length of SWNT per μm^{-2}. This density is more than sufficient to ensure that the SWNT network is above the metallic percolation threshold (1.4 – 2.4 μm_{SWNT} μm^{-2}; based on typical SWNTs lengths of 7 – 12 μm).[62] Figure 2c shows a representative micro-Raman spectrum of a pristine HD SWNT network. The peaks marked with an (*) at 303 cm^{-1}, 521 cm^{-1} and 950 cm^{-1} originate from the Si/SiO_2 substrate which are used as a reference against which other peak intensities could be compared. The presence of radial breathing modes (RBM) between 100 and 350 cm^{-1} are clearly observed, confirming the presence of SWNTs. Moreover, the *G*-peak (1585 cm^{-1}, sp^2 graphitic carbon) was *ca*. 30 times the intensity of the *D*-peak (1350 cm^{-1}), indicating that the networks are of a high quality. The small *D*-peak could arise from defect sites or a small amount of amorphous carbon.

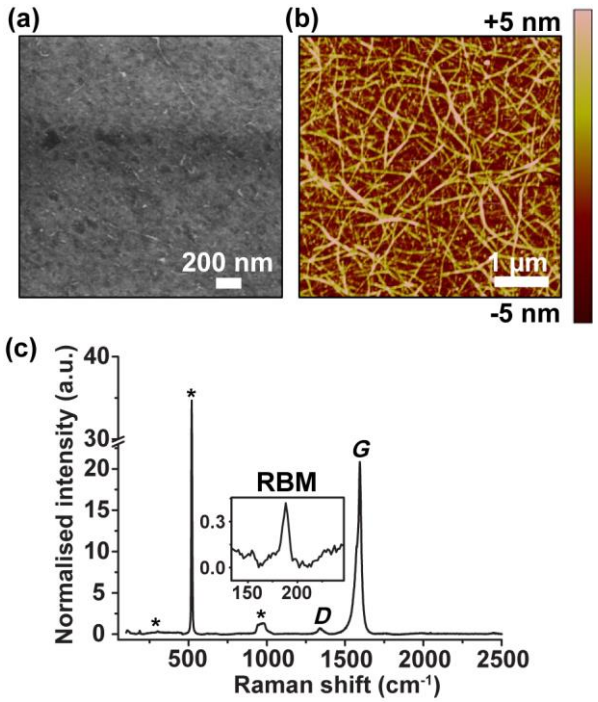

Figure 2. Typical (a) FE-SEM and (b) AFM images of a HD SWNT network. (c) Corresponding micro-Raman spectrum.

For the direct approach, $Ni(OH)_2$ NPs can be seen to precipitate uniformly on the multiply interconnected HD SWNT networks, as shown in the FE-SEM (Figure 3a) and AFM (Figure 3b) images, respectively. It is estimated (semi-quantitatively), as described in detail in **ESI Section 1,** that > 10^{-3} M concentrations of OH^- are generated close to the electrode, resulting in very high relative saturation ratios of $10^8 – 10^9$ with respect to $Ni(OH)_2$, thus promoting high nucleation rates and the formation of $Ni(OH)_2$ NPs.[12] Cross-sectional AFM height analysis (Figure 3c) reveals NP heights in the range 3 – 12 nm. The EDS data in Figure S2a and S2b, **ESI Section 1**, show no Pt signal proving that the $Ni(OH)_2$ deposition is not related to a Pt wire used as a CE.

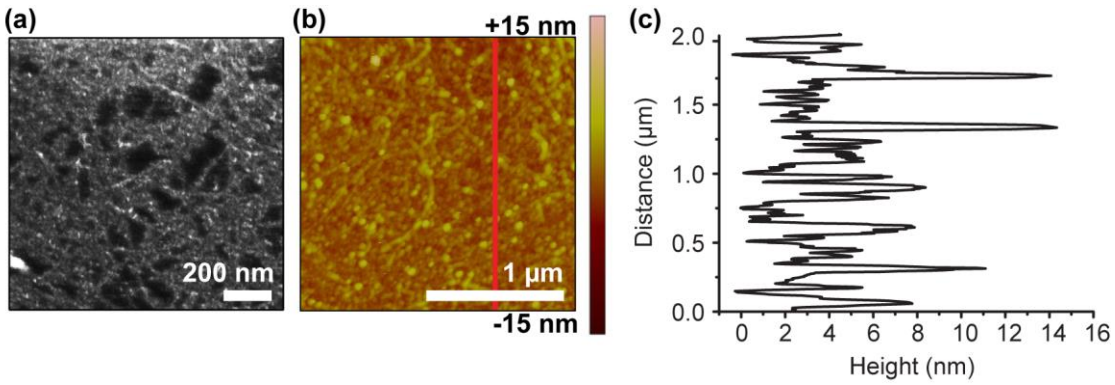

Figure 3. Typical (a) FE-SEM and (b) AFM images of a HD SWNT network electrode modified with $Ni(OH)_2$ (deposition parameters 5 s at -1.5 V *vs*. Ag/AgCl in 10 mM $(Ni(NO_3)_2$ solution). (c) AFM cross sectional height analysis (red line in b) of the NPs.

For the indirect approach, typical FE-SEM and higher resolution AFM images of the SWNT electrode surface recorded after Ni electrodeposition, but prior to electrochemical cycling in basic electrolyte are shown in Figures 4(ai) and 4(bi) respectively. The Ni NPs were widely distributed over the HD SWNTs. Due to the reduced lattice spacing and more dense nature of the native metal, Ni NPs provide better contrast against the SWNTs in FE-SEM than the $Ni(OH)_2$ NPs (Figure 3a).[63] As determined by AFM, Ni NPs of heights in the range 3 – 25 nm were formed during the initial electrodeposition process. The Ni NPs were then converted to $Ni(OH)_2$ by potential cycling, in 0.1 M KOH, sweeping from +0.1 V to +0.5 V at a potential scan rate of 5 mV s^{-1}, as shown in Figure S1c, **ESI Section 1**. The current decreased significantly for the first seven cycles as a result of the transformation of metal Ni to $Ni(OH)_2$, and remained relatively stable with further cycles.[64] Figures 4(a,b) show typical FE-SEM and AFM images of the surface after (ii) 1 and (iii) 10 cycles. NPs of 6 – 75 nm and 25 – 80 nm in height were found after 1 and 10 cycles, respectively, clearly showing the size of the NPs increases with increasing cycle number (Figure 4c). However, it is difficult to determine the actual size of the NPs, as there is

evidence of NP agglomeration on the SWNTs. Hence, HR-TEM (*vide infra*) was carried out to provide a more detailed analysis of the NPs formed.

Note that further voltammetric cycling resulted in even larger NPs, as shown in Figure 4(a, b iv) where the Ni NPs were subjected to 50 voltammetric cycles in 0.1 M KOH. Particle heights of 40 – 130 nm were determined using AFM cross sectional analysis. These data indicate that an electrochemically-induced Ostwald-ripening or agglomeration process likely operates during potential cycling that has to be controlled to avoid particles becoming too large. For electrocatalytic studies, samples with smaller NPs were of interest (due to enhanced mass action), i.e. those formed after 10 cycles (*vide infra*).

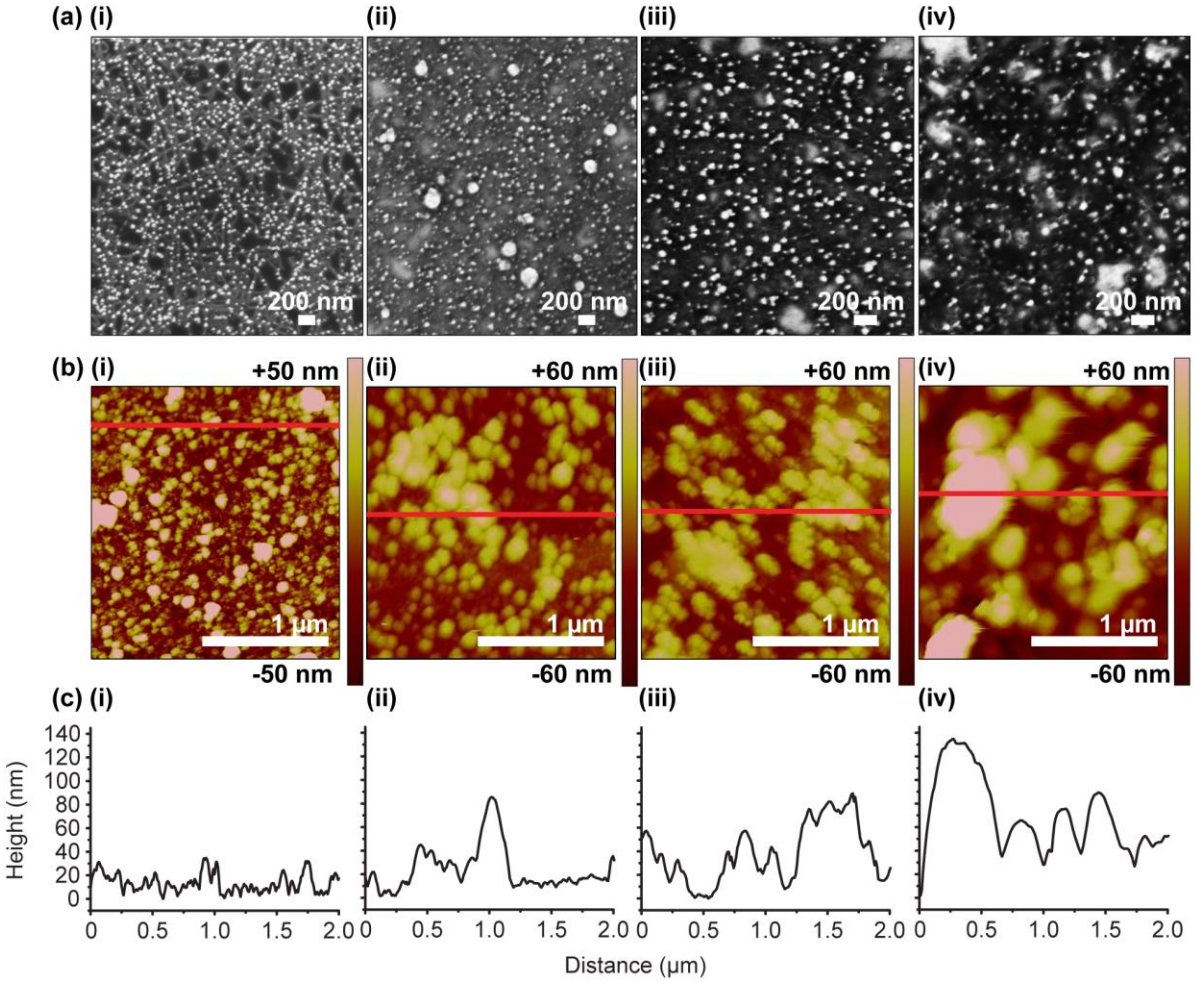

Figure 4. Typical (a) FE-SEM and (b) AFM images of HD SWNT network electrode with Ni NPs (formed by electrodeposition at -1.5 V for 5 s in 10 mM $NiSO_4$ solution) (i) before and after (ii) 1 cycle, (iii) 10 cycles and (iv) 50 cycles in 0.1 M KOH. (c) Corresponding height cross sections of the NPs.

HR-TEM analysis of the $Ni(OH)_2$ NPs is shown in Figures 5a-c (direct approach) and Figures 5d-f (indirect approach, 10 cycles). The preparation procedure for HR-TEM analysis resulted in significant NP agglomeration (as shown in Figures 5a,d) but had the advantage that it was possible to focus on individual particles within the agglomerate to provide more information on individual NP size. For the direct approach, HR-TEM shows the smallest crystallites of $Ni(OH)_2$ were around 5 nm in diameter, whilst the typical size of $Ni(OH)_2$ NPs was 10 nm, as shown in Figures 5a-b, in agreement with the AFM data (Figure 3b,c). For the indirect approach, HR-TEM shows the smallest crystallites were *ca.* 3 nm in diameter, with a typical size of 5 nm observed, as shown in Figures 5d-e, indicating that the larger sized NPs observed by AFM analysis (Figures 4b, c (ii-iv)) are due to the agglomeration of smaller NPs.

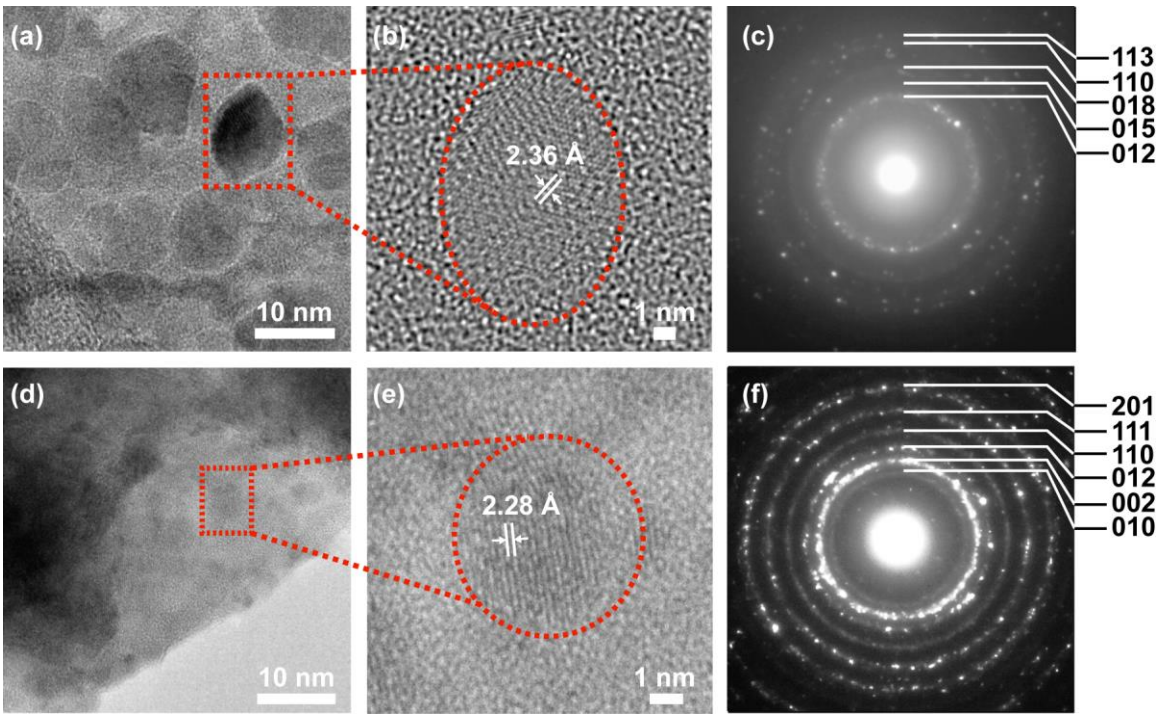

Figure 5. Typical (a, d) HR-TEM images and (c, f) SAED patterns of modified HD SWNT network electrode with $Ni(OH)_2$ NPs by the (a-c) direct and (d-f) indirect approaches.

SAED was performed on NP agglomerates that were in the holes of the supporting lacey carbon, in order to avoid carbon background interference in the TEM analysis. SAED of $Ni(OH)_2$ produced by the direct method indicated the formation of α-phase $Ni(OH)_2$ (Figure 5c; Joint Committee on Powder Diffraction Standards (JCPDS) 380715), whilst β-phase $Ni(OH)_2$ (Figure 5f; JCPDS 140117) was observed for the indirect method. Figure 6a and b show a schematic diagram representing the α and β phases of $Ni(OH)_2$, respectively.[65] Figure 6b clearly shows that the β phase (inter-sheet (001) distance, c_o = 4.60 Å) adopts a more close packed (de-hydrated) structure compared to the more disordered (c_o = 7.60 Å) hydrated α phase (Figure 6a).[65-67] For the direct approach, it is likely that the rapid precipitation process in the presence of Ni^{2+} and supersaturated concentrations of OH^- (generated electrochemically) is responsible for α-phase formation, favoring the formation of disordered α-$Ni(OH)_2$ (kinetically-driven process).

For the indirect approach, as the initial electrodeposited metallic Ni has a face-centered cubic (close packed) structure,[68] electrochemically conversion of Ni NPs to β-$Ni(OH)_2$ appears to be favored as β-phase $Ni(OH)_2$ has a similar close-packed structure. Furthermore, the slow process using potential cycling is also likely to favor the formation of the thermodynamically stable β-phase $Ni(OH)_2$.[65]

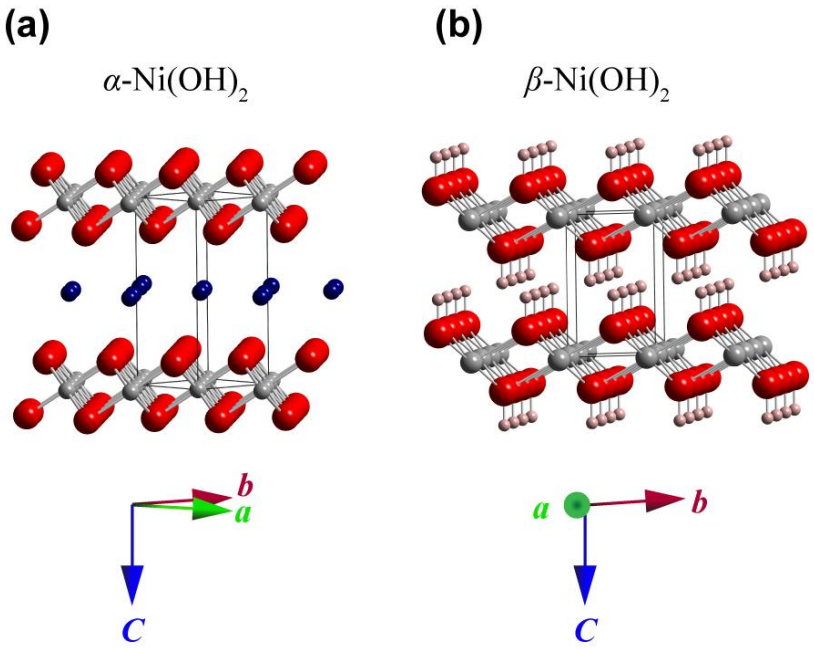

Figure 6. Schematic representation of the (a) α-$Ni(OH)_2$ phase (small grey spheres, Ni^{2+}; large red spheres, OH^-; medium size blue spheres, H_2O positions) and (b) β-$Ni(OH)_2$ phase (medium grey spheres, Ni^{2+}; large red spheres, O^{2-}; small pink spheres, H^+). In the first structure, H^+ is omitted for clarity.[65]

Figures 5b and e show the HR-TEM of a selected NP (n = 3) and the corresponding SAED images (Figures 5c and f); for an α-$Ni(OH)_2$ NP (b,c) and β-phase $Ni(OH)_2$ NP (e,f). Note the SAED sample size is ~ 675 nm, and therefore the area around the NP is also sampled. From the HR-TEM images, lattice fringes indicate d spacings of 2.36 Å for the α-$Ni(OH)_2$ NP and 2.28 Å for the β-$Ni(OH)_2$ NP. These d spacings correspond to the (015) and (002) planes, identified

using SAED, of the α and β phase $Ni(OH)_2$ NP, respectively, as provided by Figure 5c,f and the JCPDS.

MOR and EOR on $Ni(OH)_2$ NP Modified SWNT Network Electrodes

CVs were first recorded in the potential range +0.1 V to +0.55 V, on both the α and β phase $Ni(OH)_2$ modified SWNT electrodes (prepared by the direct and indirect approach, respectively) by cycling in 0.1 M KOH at 5 mV s^{-1} to estimate the amount of electroactive $Ni(OH)_2$, as shown in Figure 7. For both cases, the charge associated with Q_{ox} (oxidation of $Ni(OH)_2$; shaded area under the anodic peaks in Figure 7) is greater than the charge associated with Q_{red} (reduction of NiOOH), with Q_{ox}/Q_{red} values of 1.4 and 2.5 determined for the α-phase and β-phase $Ni(OH)_2$ NPs respectively. This is likely to be due to the fact that highly electrocatalytic NiOOH can also oxidize adsorbed OH^-, leading to the evolution of O_2 and reduction of NiOOH back to $Ni(OH)_2$. This means there are less NiOOH sites available for electrochemical reduction on the return scan.[69] The effect, however, is small, and we showed in our previous work[12] on that the anodic charge correlated well with the particle size and number, assuming volumetric conversion of $Ni(OH)_2$.

The amount of electroactive $Ni(OH)_2$ (Γ /mol cm^{-2}) is thus reasonably given by:

$$\Gamma = \frac{Q_{ox}}{nFA} \qquad (2)$$

where n is the number of electrons (n = 1), F is the Faraday constant and A is the area of the capillary opening. Given Q_{ox} values of 24.5 nC and 7.4 nC for the α-phase and β-phase $Ni(OH)_2$ respectively, Γ values of 9 ± 1 nmol cm^{-2} and 3 ± 1 nmol cm^{-2} were obtained. Given the slight enhancement of the charge on the forward sweep compared to the reverse sweep, these are

maximum values for the amount of electrodeposited $Ni(OH)_2$, and hence the specific activity values that follow are minimum values.

For α-$Ni(OH)_2$ oxidation, the oxidation peak lies 60 mV less positive than that for β-$Ni(OH)_2$ oxidation. Upon oxidation the α-$Ni(OH)_2$ transforms to γ-NiOOH,[70] the latter has a higher oxidation state (+3.5)[71] and nearly identical c_o parameter to α-$Ni(OH)_2$.[72] In contrast, β-$Ni(OH)_2$ transforms to β-NiOOH (+3 oxidation state), which only slowly transforms to γ-NiOOH (with a resulting volume change) upon prolonged (repeated) cycling.[11] In order to maintain charge neutrality during redox cycling, it is important that ions/solvent molecules can penetrate the layered $Ni(OH)_2$ structure (Figure 6); thus, as ion/solvent transfer can occur more freely in the disordered α-$Ni(OH)_2$/γ-NiOOH phase structures than in the corresponding β-phase structures,[73] this could be a likely cause of the observed differences in the CV responses in Figure 7.

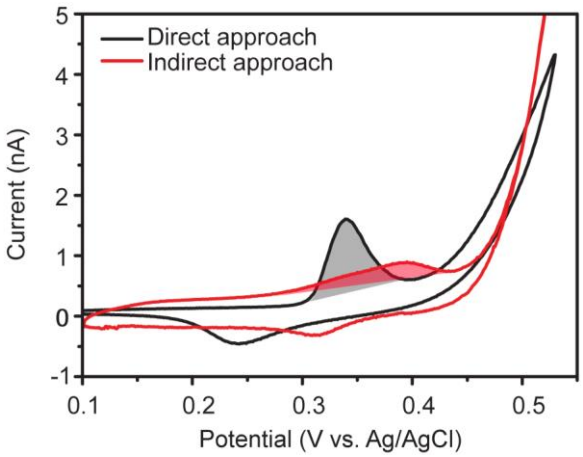

Figure 7. Typical CVs recorded using the MCEM with a capillary of 60 µm diameter in 0.1 M KOH, using a $Ni(OH)_2$ modified SWNT network electrode by the direct and indirect approaches. The potential scan rate is 5 mV s^{-1}.

The two different $Ni(OH)_2$ structures were investigated for their electrocatalytic response towards the MOR and EOR. CV measurements, at a potential scan rate of 5 mV s^{-1}, over the potential range +0.1 V to +0.55 V, were carried out in 0.5 M MeOH and 0.5 M EtOH, respectively in 0.1 M KOH. For comparison to literature values, currents were normalized by the mass of electroactive $Ni(OH)_2$ electrodeposited on the SWNT network electrode, to provide a value for specific activity (current / mass = A $g_{Ni(OH)_2}^{-1}$):

$$\text{specific activity} = \frac{inF}{Q_{ox}M_{Ni(OH)_2}} \tag{3}$$

where i is the current and $M_{Ni(OH)_2}$ is the molar mass of $Ni(OH)_2$. The calculated masses of electroactive material were 23.6 pg and 7.0 pg for α-$Ni(OH)_2$ and β-$Ni(OH)_2$, respectively. Note that the MOR and EOR responses for pristine SWNT network electrodes were negligible, even when doubling the alcohol concentration to 1 M, as shown in Figures 8a (inset). These data indicate that a bare SWNT network electrode is ineffective towards the electrochemical oxidation of alcohols, within this potential range.

For α-$Ni(OH)_2$, the forward scans in Figures 8a-b show a small anodic peak current (1) at +0.28 V and +0.31 V, followed by the appearance of larger (2) current peaks at +0.41 V and +0.48 V in the presence of EtOH and MeOH, respectively. For the reverse scan a cathodic peak current is observed at +0.20 V, for both alcohols. Peak 1 is the characteristic signal for the oxidation of $Ni(OH)_2$ to NiOOH. The second larger current peak is due to the oxidation of the alcohol, catalyzed by NiOOH, occurring at +0.3 V and +0.33 V for EtOH and MeOH, respectively. Compared to cycling in 0.1 M KOH alone, Figure 8a shows *ca*. 40 times increase in the peak current density for the EOR, which equates to a specific activity of ~3.7 kA g^{-1} and *ca*. 30 times increase in the peak current density for the MOR, which is a specific activity of ~2.8 kA

g^{-1} (Figure 8b). These values are higher than recent reports using nanostructured catalysts on carbon supports, as shown in Table 1. The small peak observed on the back scan for both the EOR and MOR, is attributed to the reduction of adsorbed intermediates (carbonaceous species not fully oxidized in the forward scan).[74]

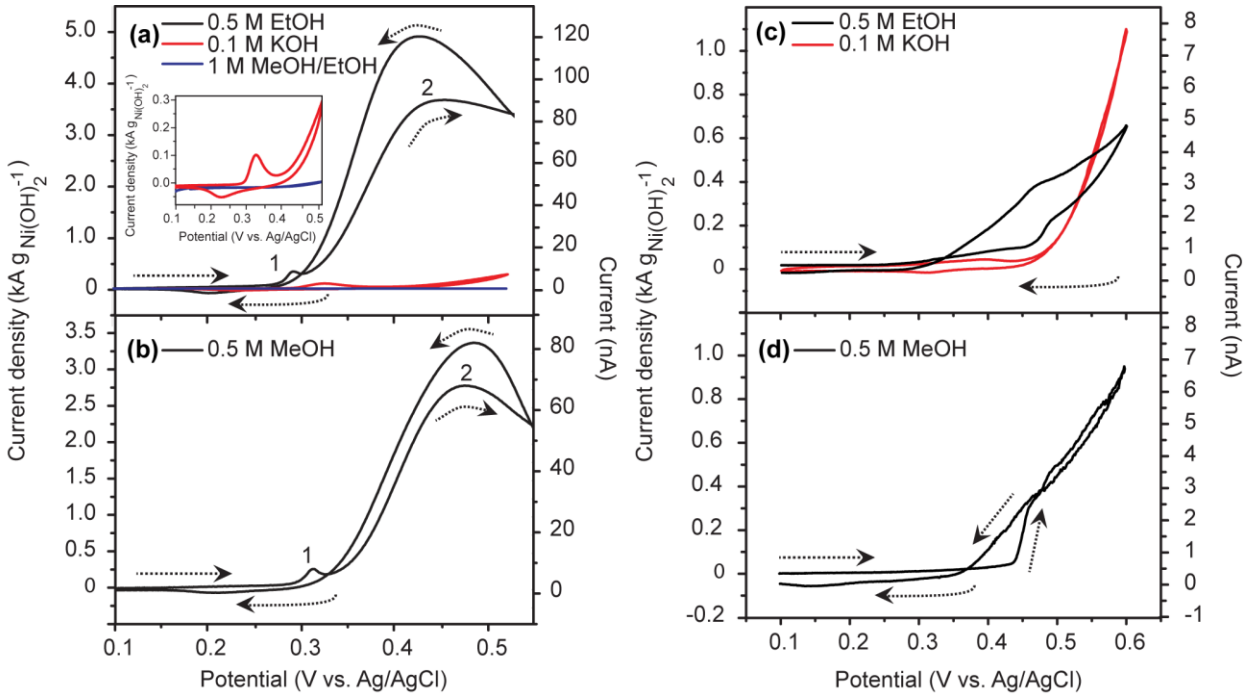

Figure 8. CVs at $Ni(OH)_2$ NP-modified SWNT network electrodes using the (a, b) direct and (c, d) indirect approach in a solution of 0.1 M KOH (red) with (a, c) 0.5 M EtOH and (b, d) 0.5 M MeOH (black). Inset: Magnification of the CVs of bare SWNT network electrode (blue) in 0.1 M KOH solution containing 1 M EtOH + 1 M MeOH and $Ni(OH)_2$/SWNT in 0.1 M KOH (red). The potential scan rate was 5 mV s^{-1}.

For β-$Ni(OH)_2$, Figures 8c-d show the CVs recorded from +0.1 V to +0.60 V in the absence (0.1 M KOH only) and presence of 0.5 M EtOH (Figure 8c) and MeOH (Figure 8d). In contrast to the data in Figure 8a, it is not possible to differentiate between oxidation of the $Ni(OH)_2$ and oxidation of the alcohol, instead one single oxidation wave is seen, which itself is not clearly defined. Therefore, it is difficult to define precisely an onset potential for AOR,

although the current can be seen to begin increasing from a ~ zero baseline *ca.* +0.34 V and +0.37 V in the presence of EtOH and MeOH, respectively. The CV characteristic is most likely due to the sluggish kinetics of the β-$Ni(OH)_2$ to β-NiOOH conversion and the oxidation of the alcohol. By taking the current at +0.47 V for the EOR and +0.45 V for the MOR, SA values of ~0.4 kA g^{-1} and ~0.3 kA g^{-1} are estimated for the EOR and MOR, respectively. These values are *ca*. 9 times smaller than for the NPs obtained by the direct approach. Cycling β-$Ni(OH)_2$ NPs reduces the catalytic efficiency even further, as shown by the CV in Figure S3, **ESI Section 2**, for a β-$Ni(OH)_2$/SWNT in 0.5 M EtOH, with the electrode prepared by 50, rather than 10 potential cycles of electrodeposited Ni NPs in 0.1 M KOH (Figure 4vi).

Overall, it is apparent that α-$Ni(OH)_2$ produced by the direct approach exhibits faster kinetics and superior electrocatalytic (oxidizing) properties, compared to β-$Ni(OH)_2$ produced by the indirect approach. The improved performance of the α-phase over the β-phase could be due to several factors including: (i) the more disordered structure of α-$Ni(OH)_2$/γ-NiOOH which enables more facile ion-solvent intercalation, to maintain charge neutrality during electrocatalysis;[75] (ii) γ-NiOOH has a higher oxidation state than β-NiOOH and, in principle, could act as a more effective electro-oxidation catalyst.[70-72]

Table 1. Nanostructured catalysts for MOR and EOR.

Electrode modification	Electrolyte, Scan rate	Maximum catalytic current ($A\ g_{Ni(OH)2}^{-1}$)		Ref.
		MeOH	EtOH	
Pt-Ru-Ni-P/Carbon supported	0.5 M H_2SO_4 and 0.5 M CH_3OH, 50 mV s^{-1}	459	-	[76]

Pt-TiO_2/Graphene composites	0.5 M H_2SO_4 and 1 M CH_3OH, 100 mV s^{-1}	1354	-	[77]
Pt-Ag/Glassy carbon electrode	0.5 M H_2SO_4 and 1 M CH_3OH, 50 mV s^{-1}	400	-	[78]
Pt-Ru/Carbon supported	0.1 M $HClO_4$ and 0.5 M CH_3OH	300	-	[79]
Pd-Ag/Graphene oxide	1 M KOH and 1 M CH_3OH, 1 M CH_2CH_3OH, 50 mV s^{-1}	600	1500	[80]
Cu-Pt-Pd/Carbon supported	0.5 M H_2SO_4 and 1 M CH_3OH, 1 M CH_2CH_3OH, 50 mV s^{-1}	700	1200	[81]
Pd-Cu-Sn/CNTs	1 M KOH and 0.5 M CH_3OH, 0.5 M CH_2CH_3OH, 50 mV s^{-1}	396	873	[82]
$Ni(OH)_2$/Boron-doped diamond	0.1 M KOH and 0.5 M CH_3OH, 0.5 M CH_2CH_3OH, 5 mV s^{-1}	990	1010	[12]
$Ni(OH)_2$/HD SWNT	0.1 M KOH and 0.5 M CH_3OH, 0.5 M CH_2CH_3OH, 5 mV s^{-1}	2800	3700	This work

CONCLUSIONS

The studies herein have revealed detailed information on the structure and electrocatalytic activity of $Ni(OH)_2$ NPs produced by two different electrochemical approaches on HD SWNTs. For the direct approach, $Ni(OH)_2$ NPs were formed by electro-generating relatively high concentrations of OH^- at the electrode surface in the presence of Ni^{2+}. For the

indirect approach, Ni NPs were first electrodeposited on the SWNTs and then electrochemically transformed to $Ni(OH)_2$ by potential cycling in alkaline media.

NP distribution was investigated using FE-SEM, whilst AFM was employed to provide quantitative information on NP size. AFM revealed individual NPs for the direct approach, of size in the range 3 – 12 nm. For the indirect approach, AFM indicated that NP aggregation was a potential problem, revealing a wide size distribution of 25 – 80 nm in the height of nanostructures. HR-TEM was used to provide higher resolution information on the NP deposits. This revealed typical NP crystallites of sizes 10 nm and 5 nm for the direct and indirect approaches, respectively. The latter data supported the idea that the larger nanostructured material, as observed by AFM, was produced by the aggregation of smaller NPs.

A key part of our study was to determine the crystallography of individual NPs using SAED in the HR-TEM. It was possible to assign NPs formed by direct deposition to the disordered (hydrated) α-phase and those formed via indirect deposition to the ordered (de-hydrated) β-phase. The different phases formed by these methods can be rationalized because in the direct approach extremely high supersaturations are generated resulted in the immediate precipitation of the kinetically favored α-phase of $Ni(OH)_2$. In contrast, the potential cycling approach involves a slow conversion of Ni to $Ni(OH)_2$, leading to the more thermodynamically favored β-phase of $Ni(OH)_2$.

α-$Ni(OH)_2$ NPs formed via the direct approach, performed remarkably well in terms of the high specific activities for the MOR (~2.8 kA g^{-1}) and EOR (~3.7 kA g^{-1}), for 0.5 M of alcohol, compared to β-$Ni(OH)_2$ NPs for the MOR (~0.3 kA g^{-1}) and EOR (~0.4 kA g^{-1}) respectively. This difference was mainly attributed to the more disordered nature of α-$Ni(OH)_2$ /γ-NiOOH, compared to β-$Ni(OH)_2$/β-NiOOH, leading to more ready ion-solvent intercalation

during electrocatalysis in the former case. Furthermore, γ-NiOOH has a higher oxidation state than β-NiOOH which could make it more effective as a catalyst for electro-oxidation .

Finally, it is important to highlight the MCEM as approach to quickly screen electrocatalysts and that our studies have allowed the study of SWNT-$Ni(OH)_2$ nanostructured electrodes without any need for an additional support electrode so that the intrinsic activity of this novel composite is investigated without complications from a substrate electrode.

Supporting Information. Section S1. $Ni(OH)_2$ NPs production via the direct and indirect approach. Section S2. EOR on β-$Ni(OH)_2$ NPs modified SWNT network electrodes.

ACKNOWLEDGMENTS

The authors thank Dr. Yang-Rae Kim, Anatolii Cuharuc, David Perry and Ashley Page for fruitful discussions. This work was part-supported by the European Research Council (ERC-2009-AdG 247143-QUANTIF) (PRU and RAL). JVM thanks the Royal Society for the award of an Industry Fellowship. SPE thanks the University of Warwick for the award of a Chancellor's International Scholarship. DL acknowledges support from the Warwick-China Scholarship Council for a joint scholarship and MV thanks Brazilian agencies CAPES, CNPq and Fundacao Araucaria (308/2014) for funding and awards.

REFERENCES

(1) Ghenciu, A. F. Review of Fuel Processing Catalysts for Hydrogen Production in PEM Fuel Cell Systems. *Curr. Opin. Solid St. M.* **2002**, *6*, 389-399.

(2) Wang, J.; Musameh, M. Carbon Nanotube/Teflon Composite Electrochemical Sensors and Biosensors. *Anal. Chem.* **2003**, *75*, 2075-2079.

(3) Miller, T. S.; Sansuk, S.; E, S. P.; Lai, S. C. S.; Macpherson, J. V.; Unwin, P. R. Pt Nanoparticle Modified Single Walled Carbon Nanotube Network Electrodes for Electrocatalysis: Control of the Specific Surface Area over Three Orders of Magnitude. *Catal. Today* **2014**, *244*, 136-145.

(4) Li, Y.; Gao, W.; Ci, L.; Wang, C.; Ajayan, P. M. Catalytic Performance of Pt Nanoparticles on Reduced Graphene Oxide for Methanol Electro-Oxidation. *Carbon* **2010**, *48*, 1124-1130.

(5) Gao, M. R.; Sheng, W. C.; Zhuang, Z. B.; Fang, Q. R.; Gu, S.; Jiang, J.; Yan, Y. S. Efficient Water Oxidation Using Nanostructured α-Nickel-Hydroxide as an Electrocatalyst. *J. Am. Chem. Soc.* **2014**, *136*, 7077-7084.

(6) Gong, M., et al. Nanoscale Nickel Oxide/Nickel Heterostructures for Active Hydrogen Evolution Electrocatalysis. *Nat. Commun.* **2014**, *5*, 4695.

(7) Li, H. B.; Yu, M. H.; Wang, F. X.; Liu, P.; Liang, Y.; Xiao, J.; Wang, C. X.; Tong, Y. X.; Yang, G. W. Amorphous Nickel Hydroxide Nanospheres with Ultrahigh Capacitance and Energy Density as Electrochemical Pseudocapacitor Materials. *Nat. Commun.* **2013**, *4*, 1894.

(8) Mu, Y.; Jia, D.; He, Y.; Miao, Y.; Wu, H.-L. Nano Nickel Oxide Modified Non-Enzymatic Glucose Sensors with Enhanced Sensitivity through an Electrochemical Process Strategy at High Potential. *Biosens. Bioelectron.* **2011**, *26*, 2948-2952.

(9) Casas-Cabanas, M.; Canales-Vazquez, J.; Rodriguez-Carvajal, J.; Rosa Palacin, M. Deciphering the Structural Transformations During Nickel Oxyhydroxide Electrode Operation. *J. Am. Chem. Soc.* **2007**, *129*, 5840-5842.

(10) Liu, J.; Chen, M.; Zhang, L.; Jiang, J.; Yan, J.; Huang, Y.; Lin, J.; Fan, H. J.; Shen, Z. X. A Flexible Alkaline Rechargeable Ni/Fe Battery Based on Graphene Foam/Carbon Nanotubes Hybrid Film. *Nano Lett.* **2014**, *14*, 7180-7187.

(11) Oliva, P.; Leonardi, J.; Laurent, J. F.; Delmas, C.; Braconnier, J. J.; Figlarz, M.; Fievet, F.; Deguibert, A. Review of the Structure and the Electrochemistry of Nickel Hydroxides and Oxy-Hydroxides. *J. Power Sources* **1982**, *8*, 229-255.

(12) Hutton, L. A.; Vidotti, M.; Patel, A. N.; Newton, M. E.; Unwin, P. R.; Macpherson, J. V. Electrodeposition of Nickel Hydroxide Nanoparticles on Boron-Doped Diamond Electrodes for Oxidative Electrocatalysis. *J. Phys. Chem. C* **2011**, *115*, 1649-1658.

(13) Reim, R. E.; Vaneffen, R. M. Determination of Carbohydrates by Liquid-Chromatography with Oxidation at a Nickel(III) Oxide Electrode. *Anal. Chem.* **1986**, *58*, 3203-3207.

(14) Dai, W.; Li, H.; Li, M.; Li, C.; Wu, X.; Yang, B. Electrochemical Imprinted Polycrystalline Nickel-Nickel Oxide Half-Nanotube-Modified Boron-Doped Diamond Electrode for the Detection of $_{L}$-Serine. *ACS Appl. Mater. Inter.* **2015**, 7, 22858-22867.

(15) Kraeutler, B.; Bard, A. J. Heterogeneous Photocatalytic Preparation of Supported Catalysts-Photodeposition of Platinum on TiO_2 Powder and Other Substrates. *J. Am. Chem. Soc.* **1978**, *100*, 4317-4318.

(16) Kleijn, S. E. F.; Lai, S. C. S.; Koper, M. T. M.; Unwin, P. R. Electrochemistry of Nanoparticles. *Angew. Chem. Int. Ed.* **2014**, *53*, 3558-3586.

(17) Li, W. Z.; Liang, C. H.; Zhou, W. J.; Qiu, J. S.; Zhou, Z. H.; Sun, G. Q.; Xin, Q. Preparation and Characterization of Multiwalled Carbon Nanotube-Supported Platinum for Cathode Catalysts of Direct Methanol Fuel Cells. *J. Phys. Chem. B* **2003**, *107*, 6292-6299.

(18) Mu, Y. Y.; Liang, H. P.; Hu, J. S.; Jiang, L.; Wan, L. J. Controllable Pt Nanoparticle Deposition on Carbon Nanotubes as an Anode Catalyst for Direct Methanol Fuel Cells. *J. Phys. Chem. B* **2005**, *109*, 22212-22216.

(19) Corso, B. L.; Perez, I.; Sheps, T.; Sims, P. C.; Gül, O. T.; Collins, P. G. Electrochemical Charge-Transfer Resistance in Carbon Nanotube Composites. *Nano Lett.* **2014**, *14*, 1329-1336.

(20) Güell, A. G.; Ebejer, N.; Snowden, M. E.; McKelvey, K.; Macpherson, J. V.; Unwin, P. R. Quantitative Nanoscale Visualization of Heterogeneous Electron Transfer Rates in 2D Carbon Nanotube Networks. *P. Natl. Acad. Sci. USA* **2012**, *109*, 11487-11492.

(21) Heller, I.; Kong, J.; Heering, H. A.; Williams, K. A.; Lemay, S. G.; Dekker, C. Individual Single-Walled Carbon Nanotubes as Nanoelectrodes for Electrochemistry. *Nano Lett.* **2005**, *5*, 137-142.

(22) Kongkanand, A.; Kuwabata, S.; Girishkumar, G.; Kamat, P. Single-Wall Carbon Nanotubes Supported Platinum Nanoparticles with Improved Electrocatalytic Activity for Oxygen Reduction Reaction. *Langmuir* **2006**, *22*, 2392-2396.

(23) Joo, S. H.; Choi, S. J.; Oh, I.; Kwak, J.; Liu, Z.; Terasaki, O.; Ryoo, R. Ordered Nanoporous Arrays of Carbon Supporting High Dispersions of Platinum Nanoparticles. *Nature* **2001**, *412*, 169-172.

(24) Zhou, X.; Xia, Z.; Zhang, Z.; Ma, Y.; Qu, Y. One-Step Synthesis of Multi-Walled Carbon Nanotubes/Ultra-Thin $Ni(OH)_2$ Nanoplate Composite as Efficient Catalysts for Water Oxidation. *J. Mater. Chem. A* **2014**, *2*, 11799-11806.

(25) Yang, M. H.; Yang, Y. H.; Liu, Y. L.; Shen, G. L.; Yu, R. Q. Platinum Nanoparticles-Doped Sol-Gel/Carbon Nanotubes Composite Electrochemical Sensors and Biosensors. *Biosens. Bioelectron.* **2006**, *21*, 1125-1131.

(26) Zhang, X.; Zhang, B.; Li, X.-D.; Ma, L.-X.; Zhang, J.-W. Sonochemical Synthesis of Hollow Pt Alloy Nanostructures on Carbon Nanotubes with Enhanced Electrocatalytic Activity for Methanol Oxidation Reaction. *Int. J. Hydrogen Energ.* **2015**, *40*, 14416-14420.

(27) Lu, Q. Y.; Gao, F.; Zhao, D. Y. One-Step Synthesis and Assembly of Copper Sulfide Nanoparticles to Nanowires, Nanotubes, and Nanovesicles by a Simple Organic Amine-Assisted Hydrothermal Process. *Nano Lett.* **2002**, *2*, 725-728.

(28) Day, T. M.; Unwin, P. R.; Macpherson, J. V. Factors Controlling the Electrodeposition of Metal Nanoparticles on Pristine Single Walled Carbon Nanotubes. *Nano Lett.* **2007**, *7*, 51-57.

(29) Miller, T. S.; Macpherson, J. V.; Unwin, P. R. Dual-Electrode Measurements in a Meniscus Microcapillary Electrochemical Cell Using a High Aspect Ratio Carbon Fibre Ultramicroelectrode. *J. Electroanal. Chem.* **2014**, *729*, 80-86.

(30) Asgari, M.; Maragheh, M. G.; Davarkhah, R.; Lohrasbi, E. Methanol Electrooxidation on the Nickel Oxide Nanoparticles/Multi-Walled Carbon Nanotubes Modified Glassy Carbon Electrode Prepared Using Pulsed Electrodeposition. *J. Electrochem. Soc.* **2011**, *158*, K225-K229.

(31) Xu, C.; Sun, J.; Gao, L. Large Scale Synthesis of Nickel Oxide/Multiwalled Carbon Nanotube Composites by Direct Thermal Decomposition and Their Lithium Storage Properties. *J. Power Sources* **2011**, *196*, 5138-5142.

(32) Shi, Z. J.; Lian, Y. F.; Zhou, X. H.; Gu, Z. N.; Zhang, Y. G.; Iijima, S.; Zhou, L. X.; Yue, K. T.; Zhang, S. L. Mass-Production of Single-Wall Carbon Nanotubes by Arc Discharge Method. *Carbon* **1999**, *37*, 1449-1453.

(33) Munoz, E.; Maser, W. K.; Benito, A. M.; Martinez, M. T.; de la Fuente, G. F.; Maniette, Y.; Righi, A.; Anglaret, E.; Sauvajol, J. L. Gas and Pressure Effects on the Production of Single-Walled Carbon Nanotubes by Laser Ablation. *Carbon* **2000**, *38*, 1445-1451.

(34) Huang, S. M.; Woodson, M.; Smalley, R.; Liu, J. Growth Mechanism of Oriented Long Single Walled Carbon Nanotubes Using "Fast-Heating" Chemical Vapor Deposition Process. *Nano Lett.* **2004**, *4*, 1025-1028.

(35) Hiura, H.; Ebbesen, T. W.; Tanigaki, K. Opening and Purification of Carbon Nanotubes in High Yields. *Adv. Mater.* **1995**, *7*, 275-276.

(36) Yuge, R.; Toyama, K.; Ichihashi, T.; Ohkawa, T.; Aoki, Y.; Manako, T. Characterization and Field Emission Properties of Multi-Walled Carbon Nanotubes with Fine Crystallinity Prepared by CO_2 Laser Ablation. *Appl. Surf. Sci.* **2012**, *258*, 6958-6962.

(37) Pumera, M., Carbon Nanotubes Contain Residual Metal Catalyst Nanoparticles Even after Washing with Nitric Acid at Elevated Temperature Because These Metal Nanoparticles Are Sheathed by Several Graphene Sheets. *Langmuir* **2007**, *23*, 6453-6458.

(38) Rosca, I. D.; Watari, F.; Uo, M.; Akaska, T. Oxidation of Multiwalled Carbon Nanotubes by Nitric Acid. *Carbon* **2005**, *43*, 3124-3131.

(39) Pumera, M.; Iwai, H. Multicomponent Metallic Impurities and Their Influence Upon the Electrochemistry of Carbon Nanotubes. *J. Phys. Chem. C* **2009**, *113*, 4401-4405.

(40) Fan, Y. W.; Goldsmith, B. R.; Collins, P. G. Identifying and Counting Point Defects in Carbon Nanotubes. *Nat. Mater.* **2005**, *4*, 906-911.

(41) Dumitrescu, I.; Wilson, N. R.; Macpherson, J. V. Functionalizing Single-Walled Carbon Nanotube Networks: Effect on Electrical and Electrochemical Properties. *J. Phys. Chem. C* **2007**, *111*, 12944-12953.

(42) Pickett, D. F.; Maloy, J. T. Micro-Electrode Studies of Electrochemically Coprecipitated Cobalt Hydroxide in Nickel-Hydroxide Electrodes. *J. Electrochem. Soc.* **1978**, *125*, 1026-1032.

(43) Corrigan, D. A. The Catalysis of the Oxygen Evolution Reaction by Iron Impurities in Thin-Film Nickel-Oxide Electrodes. *J. Electrochem. Soc.* **1987**, *134*, 377-384.

(44) Jayashree, R. S.; Kamath, P. V. Nickel Hydroxide Electrodeposition from Nickel Nitrate Solutions: Mechanistic Studies. *J. Power Sources* **2001**, *93*, 273-278.

(45) Streinz, C. C.; Hartman, A. P.; Motupally, S.; Weidner, J. W. The Effect of Current and Nickel Nitrate Concentration on the Deposition of Nickel-Hydroxide Films. *J. Electrochem. Soc.* **1995**, *142*, 1084-1089.

(46) Hu, Y. N.; Scherson, D. A. Potential-Induced Plastic Deformations of Nickel Hydrous Electrodes in Alkaline Electrolytes: An in Situ Atomic Force Microscopy Study. *J. Phys. Chem. B* **1997**, *101*, 5370-5376.

(47) Hopper, M. A.; Ord, J. L. Optical Study of Growth and Oxidation of Nickel Hydroxide Films. *J. Electrochem. Soc.* **1973**, *120*, 183-187.

(48) Wolf, J. F.; Yeh, L. S. R.; Damjanovic, A. Anodic Oxide-Films at Nickel Electrodes in Alkaline-Solutions.1. Kinetics of Growth of the Beta-$Ni(OH)_2$ Phase. *Electrochim. Acta* **1981**, *26*, 409-416.

(49) Deo, R. P.; Lawrence, N. S.; Wang, J., Electrochemical Detection of Amino Acids at Carbon Nanotube and Nickel-Carbon Nanotube Modified Electrodes. *Analyst* **2004**, *129*, 1076-1081.

(50) Liao, S. J.; Holmes, K. A.; Tsaprailis, H.; Birss, V. I. High Performance PtRulr Catalysts Supported on Carbon Nanotubes for the Anodic Oxidation of Methanol. *J. Am. Chem. Soc.* **2006**, *128*, 3504-3505.

(51) Luo, H. X.; Shi, Z. J.; Li, N. Q.; Gu, Z. N.; Zhuang, Q. K. Investigation of the Electrochemical and Electrocatalytic Behavior of Single-Wall Carbon Nanotube Film on a Glassy Carbon Electrode. *Anal. Chem.* **2001**, *73*, 915-920.

(52) Paolucci, D.; Marcaccio, M.; Bruno, C.; Paolucci, F.; Tagmatarchis, N.; Prato, M. Voltammetric Quantum Charging Capacitance Behaviour of Functionalised Carbon Nanotubes in Solution. *Electrochim. Acta* **2008**, *53*, 4059-4064.

(53) Dudin, P. V.; Unwin, P. R.; Macpherson, J. V. Electro-Oxidation of Hydrazine at Gold Nanoparticle Functionalised Single Walled Carbon Nanotube Network Ultramicroelectrodes. *Phys. Chem. Chem. Phys.* **2011**, *13*, 17146-17152.

(54) Edgeworth, J. P.; Wilson, N. R.; Macpherson, J. V. Controlled Growth and Characterization of Two-Dimensional Single-Walled Carbon-Nanotube Networks for Electrical Applications. *Small* **2007**, *3*, 860-870.

(55) Bertoncello, P.; Edgeworth, J. P.; Macpherson, J. V.; Unwin, P. R. Trace Level Cyclic Voltammetry Facilitated by Single-Walled Carbon Nanotube Network Electrodes. *J. Am. Chem. Soc.* **2007**, *129*, 10982-10983.

(56) Zhang, G.; Cuharuc, A. S.; Güell, A. G.; Unwin, P. R. Electrochemistry at Highly Oriented Pyrolytic Graphite (HOPG): Lower Limit for the Kinetics of Outer-Sphere Redox Processes and General Implications for Electron Transfer Models. *Phys. Chem. Chem. Phys.* **2015**, *17*, 11827-11838.

(57) Cuharuc, A. S.; Zhang, G.; Unwin, P. R. Electrochemistry of Ferrocene Derivatives on Highly Oriented Pyrolytic Graphite (HOPG): Quantification and Impacts of Surface Adsorption. *Phys. Chem. Chem. Phys.* **2016**, *18*, 4966-4977.

(58) Portemer, F.; Delahayevidal, A.; Figlarz, M. Characterization of Active Material Deposited at the Nickel-Hydroxide Electrode by Electrochemical Impregnation. *J. Electrochem. Soc.* **1992**, *139*, 671-678.

(59) Dudin, P. V.; Unwin, P. R.; Macpherson, J. V. Electrochemical Nucleation and Growth of Gold Nanoparticles on Single-Walled Carbon Nanotubes: New Mechanistic Insights. *J. Phys. Chem. C* **2010**, *114*, 13241-13248.

(60) Zhang, G. H.; Kirkman, P. M.; Patel, A. N.; Cuharuc, A. S.; McKelvey, K.; Unwin, P. R. Molecular Functionalization of Graphite Surfaces: Basal Plane Versus Step Edge Electrochemical Activity. *J. Am. Chem. Soc.* **2014**, *136*, 11444-11451.

(61) Güell, A. G.; Meadows, K. E.; Dudin, P. V.; Ebejer, N.; Macpherson, J. V.; Unwin, P. R. Mapping Nanoscale Electrochemistry of Individual Single-Walled Carbon Nanotubes. *Nano Lett.* **2014**, *14*, 220-224.

(62) E, S. P.; Miller, T. S.; Macpherson, J. V.; Unwin, P. R. Controlled Functionalisation of Single-Walled Carbon Nanotube Network Electrodes for the Enhanced Voltammetric Detection of Dopamine. *Phys. Chem. Chem. Phys.* **2015**, *17*, 26394-26402.

(63) Goldstein, J.; Newbury, D. E.; Echlin, P.; Joy, D. C.; Fiori, C.; Lifshin, E. *Scanning Electron Microscopy and X-Ray Microanalysis: A Text for Biologists, Materials Scientists, and Geologists*; Springer US: New York, 2013.

(64) Fantini, M. C. A.; Gorenstein, A. Electrochromic Nickel-Hydroxide Films on Transparent Conducting Substrates. *Sol. Energ. Mater.* **1987**, 16, 487-500.

(65) Hall, D. S.; Lockwood, D. J.; Bock, C.; MacDougall, B. R. Nickel Hydroxides and Related Materials: A Review of Their Structures, Synthesis and Properties. *P. Roy. Soc. A Mat.* **2015**, *471*.

(66) Song, Q. S.; Tang, Z. Y.; Guo, H. T.; Chan, S. L. I. Structural Characteristics of Nickel Hydroxide Synthesized by a Chemical Precipitation Route under Different pH Values. *J. Power Sources* **2002**, *112*, 428-434.

(67) McEwen, R. S. Crystallographic Studies on Nickel Hydroxide and Higher Nickel Oxides. *J. Phys. Chem.* **1971**, *75*, 1782-1789.

(68) Parks, E. K.; Zhu, L.; Ho, J.; Riley, S. J. The Structure of Small Nickel Clusters .2. Ni-16-Ni-28. *J. Chem. Phys.* **1995**, *102*, 7377-7389.

(69) Ayeb, A.; Notten, P. H. L. The Oxygen Evolution Kinetics in Sealed Rechargeable NiMH Batteries. *Electrochim. Acta* **2008**, *53*, 5836-5847.

(70) Cornilsen, B. C.; Shan, X. Y.; Loyselle, P. L. Structural Comparison of Nickel Electrodes and Precursor Phases. *J. Power Sources* **1990**, *29*, 453-466.

(71) Kamath, P. V.; Dixit, M.; Indira, L.; Shukla, A. K.; Kumar, V. G.; Munichandraiah, N. Stabilized α-$Ni(OH)_2$ as Electrode Material for Alkaline Secondary Cells. *J. Electrochem. Soc.* **1994**, *141*, 2956-2959.

(72) Kumar, V. G.; Munichandraiah, N.; Kamath, P. V.; Shukla, A. K. On the Performance of Stabilized α-Nickel Hydroxide as a Nickel-Positive Electrode in Alkaline Storage Batteries. *J. Power Sources* **1995**, *56*, 111-114.

(73) French, H. M.; Henderson, M. J.; Hillman, A. R.; Vieil, E. Ion and Solvent Transfer Discrimination at a Nickel Hydroxide Film Exposed to LiOH by Combined Electrochemical Quartz Crystal Microbalance (EQCM) and Probe Beam Deflection (PBD) Techniques. *J. Electroanal. Chem.* **2001**, *500*, 192-207.

(74) Maiyalagan, T.; Scott, K. Performance of Carbon Nanofiber Supported Pd-Ni Catalysts for Electro-Oxidation of Ethanol in Alkaline Medium. *J. Power Sources* **2010**, *195*, 5246-5251.

(75) McBreen J. *Nickel Hydroxides. In Handbook of Battery Materials*; Wiley-VCH Verlag GmbH & Co.KGaA.: Weinheim, Germany, 2011.

(76) Ma, Y.; Li, H.; Wang, H.; Mao, X.; Linkov, V.; Ji, S.; Gcilitshana, O. U.; Wang, R. Evolution of the Electrocatalytic Activity of Carbon-Supported Amorphous Platinum-Ruthenium-Nickel-Phosphorous Nanoparticles for Methanol Oxidation. *J. Power Sources* **2014**, *268*, 498-507.

(77) Ye, L.; Li, Z.; Zhang, L.; Lei, F.; Lin, S. A Green One-Pot Synthesis of Pt/TiO_2/Graphene Composites and Its Electro-Photo-Synergistic Catalytic Properties for Methanol Oxidation. *J. Colloid Interf. Sci.* **2014**, *433*, 156-162.

(78) Fu, G.-T.; Ma, R.-G.; Gao, X.-Q.; Chen, Y.; Tang, Y.-W.; Lu, T.-H.; Lee, J.-M. Hydrothermal Synthesis of Pt-Ag Alloy Nano-Octahedra and Their Enhanced Electrocatalytic Activity for the Methanol Oxidation Reaction. *Nanosc.* **2014**, *6*, 12310-12314.

(79) Chen, D. J.; Sun, S. G.; Tong, Y. Y. J. On the Chemistry of Activation of a Commercial Carbon-Supported PtRu Electrocatalyst for the Methanol Oxidation Reaction. *Chem. Commun.* **2014**, *50*, 12963-12965.

(80) Li, L.; Chen, M.; Huang, G.; Yang, N.; Zhang, L.; Wang, H.; Liu, Y.; Wang, W.; Gao, J. A Green Method to Prepare Pd-Ag Nanoparticles Supported on Reduced Graphene Oxide and Their Electrochemical Catalysis of Methanol and Ethanol Oxidation. *J. Power Sources* **2014**, *263*, 13-21.

(81) Sieben, J. M.; Alvarez, A. E.; Comignani, V.; Duarte, M. M. E. Methanol and Ethanol Oxidation on Carbon Supported Nanostructured Cu Core Pt-Pd Shell Electrocatalysts Synthesized via Redox Displacement. *Int. J. Hydrogen Energ.* **2014**, *39*, 11547-11556.

(82) Zhu, F.; Ma, G.; Bai, Z.; Hang, R.; Tang, B.; Zhang, Z.; Wang, X. High Activity of Carbon Nanotubes Supported Binary and Ternary Pd-Based Catalysts for Methanol, Ethanol and Formic Acid Electro-Oxidation. *J. Power Sources* **2013**, *242*, 610-620.

Table of Contents Graphic